Noname manuscript No.
(will be inserted by the editor)

A Two Level Scaling-up method for multiphase flow in porous media; numerical validation and comparison with other methods

Alain Bourgeat · **Mladen Jurak**

November 10, 2008

Abstract We present a robust and accurate strategy for upscaling two-phase flow in heterogeneous porous media composed of different rock-types. The method is tested by means of numerical simulations and compared with other upscaling methods.

Keywords Nuclear waste repository, two-phase flow, porous media, scale up, coarsening, transport migration

Contents

1 Introduction 1
2 Upscaling problem, definitions 3
3 Effective equations 5
4 Numerical implementation 8
5 Other upscaling methods 10
6 Numerical experiment results 11
7 Conclusion 18

1 Introduction

We are interested in finding macroscopic (global) properties of two-phase flow through highly heterogeneous porous media. Namely, starting from a porous media containing, at the Darcy scale (local scale) many heterogeneities concerning respectively intrinsic one-phase rock parameters and two-phase flow capillary pressure or relative permeability curves, we want to characterize the whole domain petrographic and flow

Alain Bourgeat
Université de Lyon, Université Lyon1, CNRS UMR 5208 Institut Camille Jordan, F - 69200 Villeurbanne Cedex, France
E-mail: bourgeat@mcs.univ-lyon1.fr

Mladen Jurak
Department of mathematics, University of Zagreb, Croatia, Tel.: +385 14605738, Fax: +385 14680335,
E-mail: jurak@math.hr

properties by defining global one-phase rock parameters, and global two-phase flow petrographic characteristics. The simultaneous flow of immiscible fluids in porous media occurs in a wide variety of applications from Geohydrology, Petroleum Engineering and Environment.

The most concentrated research in this field over the past four decades has focused on underground petroleum reservoirs where two-phase flow models for enhanced oil recovery are concerned with oil and water phases. Most recently, multiphase flows have generated serious interest among engineers concerned with deep geological repository for radioactive waste (see [23]); where anaerobic corrosion of the steel engineered barriers (carbon steel overpack and stainless steel envelope) of radioactive waste packages, can produce migration of hydrogen gas in the water saturated repository isolating rock, inducing groundwater flow and transport of radionuclides. In this process the two phases are water and gas (see for instance [23], [18], [10]). Nuclear waste performance assessment requires to estimate nuclides transport migration over a million of years period, through several kilometers rock formation. Ability to understand and predict underground gas migration is crucial to the design and management of reliable waste storages. This is a fairly new frontier in multiphase porous-media flows, and inherent complexity of the physics and of the petrophysic leads to governing equations for which the only practical way to produce solutions may be numerical simulation. Additional complexity is also coming from the fact that, at a fine scale (the scale of near field models), the producing gas radioactive waste packages, are surrounded by highly different porous media like concrete buffers or plugs, bentonite tunnel backfill, damaged and fractured zone, granite or argilite host rock. As a result, of this complexity and of these huge time and spatial scales, at a fine scale, any accurate and well-resolved computation requires excessive amount of computer memory and CPU time. Moreover, preliminary to opening a nuclear waste repository, performance assessment and safety analysis have to be done and submitted to the authority.

Performance assessment consists in investigating different possible configurations or scenarios with different shapes, materials and localization for the design of packages, insulating barriers, tunnel backfilling, host rock, *etc*. Safety analysis consists in estimating risk probability to each scenario by statistical simulations mainly based on Monte Carlo method. In the one hand, all the computational tasks required by performance assessment and risk analysis exceeds the limit of today's computer resources, if done on a fine scale model; in the other hand, the computational cost of each numerical simulation will be greatly reduced by predicting the large scale solutions to certain accuracy. The only practical way to produce accurate large scale numerical simulation is then to use mathematical model consistent with the whole waste repository scale. Upscaling the host rock formation and other porous media petrographic properties at the whole waste repository scale, and deriving effective equations describing the transport migration at this same scale will be a preliminary task before starting numerical simulations for performance assessment or safety analysis.

The rest of this paper is organized as follows. In Section 2 we precise the upscaling problem and its dependence on dimensionless parameters: the Péclet number and the Bond number. In Section 3 we present our upscaling procedure and its numerical implementation is described in Section 4. In Section 5 we recall other upscaling

methods used in petroleum engineering and in Section 6 we make numerical experiments showing strength and limitations of each of these methods compared to our upscaling procedure. Conclusion is given in Section 7.

2 Upscaling problem, definitions

We consider two-phase fluid flow in a porous domain Ω, possibly part of a bigger geological domain G, which at fine scale has strong heterogeneities, each individual region of heterogeneity having different intrinsic permeability and nonlinear constitutive relationship for two-phase flow. The two fluid phases are corresponding respectively to the wetting phase, ("water" in in Nuclear waste disposal performance assessment and in Oil reservoir simulation) and to the non-wetting phase ("gas" in Nuclear waste disposal performance assessment and "oil" in Oil reservoir simulation); these two phases will be denoted herein respectively by indices w and nw. For simplicity and in order to compare to existing literature, we assume flow incompressibility and immiscibility of the two phases, each phase reduced to a single component.

At each point in the domain Ω, at the Darcy scale, the one-phase porous medium parameters are the porosity ϕ, and the absolute permeability tensor K; the two-phase rock characteristics are the relative permeability curves kr_{nw}, kr_w and the capillary pressure curve p_c. Saying that the porous domain Ω is heterogeneous, at the Darcy scale, means first that the rock one-phase parameters are rapidly varying, splitting Ω in a high number of relatively small rock blocks with different intrinsic properties, and second that there is also several different rock-type, called subdomains, such that any rock-type subdomain is characterized by one set of two-phase petrographic curves. More precisely, the domain Ω is composed of n different rock-type subdomains Ω_i; $\overline{\Omega} = \cup_{i=1}^{n} \overline{\Omega}_i$. Any rock-type subdomain Ω_i may contain several fine rock blocks with different intrinsic one-phase rock properties but all these fine rock blocks are characterized by the same couple of relative permeability curves kr_{nw}^i, kr_w^i and the same capillary pressure curve p_c^i. Governing equations are given, at local scale, by mass conservation and generalized Darcy's laws for each phase, complemented by capillary pressure law:

$$\phi \frac{\partial S}{\partial t} + \operatorname{div} \mathbf{q}_w = F_w \quad \text{in} \quad Q_T, \tag{1}$$

$$-\phi \frac{\partial S}{\partial t} + \operatorname{div} \mathbf{q}_{nw} = F_{nw} \quad \text{in} \quad Q_T, \tag{2}$$

$$\mathbf{q}_w = -\mathsf{K}(x)\lambda_w(x,S)\left(\nabla p_w - \rho_w \mathbf{g}\right), \tag{3}$$

$$\mathbf{q}_{nw} = -\mathsf{K}(x)\lambda_{nw}(x,S)\left(\nabla p_{nw} - \rho_{nw} \mathbf{g}\right), \tag{4}$$

$$p_c(x,S) = p_{nw} - p_w. \tag{5}$$

In (1)-(5), $Q_T = \Omega \times (0,T)$, ϕ is fine scale porosity, S is the wetting phase saturation, $\mathbf{q}_w$, $\mathbf{q}_{nw}$ are wetting and non-wetting phases Darcy-Muskat's velocities, $\mathsf{K}(x)$ is the intrinsic fine scale permeability tensor, p_w and p_{nw} are the phase pressures, ρ_w and ρ_{nw} are phase densities and g is the gravitational acceleration vector. F_w and F_{nw} are the sources terms for each phase; in nuclear waste simulation, we are interested

essentially by the generation of the gas phase although in petroleum engineering we will consider both oil production and water injection. Capillary pressure as defined by (5) is a monotonous decreasing function of wetting phase saturation.

Due to the fact that, at fine scale, the domain Ω is composed of different rock-type subdomains, $\overline{\Omega} = \cup_{i=1}^{n} \overline{\Omega}_i$, phase mobilities λ_ξ, $\xi \in \{w, nw\}$, in (3), (4) and capillary pressure p_c in (5) have the following form:

$$\lambda_\xi(x,S) = \sum_{i=1}^{n} \frac{1}{\mu_\xi} kr_\xi^i(S)\chi_{\Omega_i}(x), \quad p_c(x,S) = \sum_{i=1}^{n} p_c^i(S)\chi_{\Omega_i}(x); \tag{6}$$

where μ_w and μ_{nw} are the phase viscosities and χ_{Ω_i} is the subdomain Ω_i characteristic function. In any $i-$th rock-type subdomain, the capillary pressure curve and the two relative permeability curves are defined on an interval $[S_{i,m}, S_{i,M}]$, $0 \leq S_{i,m} < S_{i,M} \leq 1$, corresponding to $S_{i,m}$, the irreducible wetting phase saturation, and $1 - S_{i,M}$, the irreducible non-wetting phase saturation. From these, we may then define, in all Ω, two piecewise constant irreducible saturation functions:

$$S_m(x) = \sum_{i=1}^{n} S_{i,m}\chi_{\Omega_i}(x), \quad S_M(x) = \sum_{i=1}^{n} S_{i,M}\chi_{\Omega_i}(x). \tag{7}$$

In the local model, described by equations (1)–(5), there are two different spatial scales: a *local scale* associated to l, the small rock blocks size, i.e. the heterogeneity characteristic length, and a *global scale*, associated to L, the domain Ω characteristic length. The *upscaling problem* consists of finding the fluid flow equations at the global scale, called global or effective equations, corresponding to a homogeneous porous domain, with constant one-phase rock properties and only one rock-type. Despite its simplicity these *effective equations* should capture all effects due to fine scale domain heterogeneity in a macroscopic scale representation. This global, or macroscopic, model should keep from the local scale phenomenology only what is appearing at this global scale while neglecting what was characteristic of only the fine scale.

The scaling-up method presented herein is based on the assumption that there is a separation of scale, i.e. $\varepsilon = l/L$ is a small parameter. It is well known that effective equations depend on the fluid flow regime; and, in order to characterize the flow regime globally, we note that there are three characteristic times at the global scale: the diffusion time τ_d, the convection time τ_c and the gravity leaded convection time τ_g;

$$\tau_d = \frac{L^2\mu^0}{k^0 {p_c}^0}, \quad \tau_c = \frac{L}{q^0}, \quad \tau_g = \frac{L\mu^0}{k^0 \Delta\rho g^0}. \tag{8}$$

Where μ^0, k^0, ${p_c}^0$, q^0, g^0, denote the characteristic values of: viscosity, absolute permeability, capillary pressure, flow velocity and gravity. $\Delta\rho$ is the two phases difference of mass densities. From those three characteristic times (8) two dimensionless numbers will characterize the macroscopic flow regime: the global Péclet number Pe_g and the global Bond number Bo_g;

$$Pe_g = \tau_d/\tau_c, \quad Bo_g = \tau_d/\tau_g. \tag{9}$$

At the local scale we have similarly three characteristic times (L being replaced by l in their definitions (8)) and two local dimensionless numbers: the local Péclet Pe_l and Bond Bo_l numbers. It is clear that due to the separation of scales the global and local dimensionless numbers are related by $Pe_g = Pe_l/\varepsilon$ and $Bo_g = Bo_l/\varepsilon$.

There are several different situations, depending on the ratio between the dimensionless numbers and ε. Here, we will consider the case $Pe_g = O(1) \simeq Bo_g = O(1)$; i.e., when, at the global scale, capillary diffusion and convection are of the same order. In that last situation, effective equations were derived, assuming moreover periodicity of the heterogeneities; first by formal asymptotic expansion of equations (1)–(5), in [21]; and with rigorous justification by mathematical homogenization in [8], using a "global pressure formulation" (see: [14]) of equations (1)–(5). We note that since, in that case, the global scale equations have the same form as the local scale equations, with *effective coefficients*, upscaling reduces to only computing effective parameters and curves.

The main goal of this paper is to present an efficient and accurate numerical implementation of an upscaling method for actual situations with high oscillations in the flow field corresponding to high permeability contrasts in different regions. This is done by first generalizing the periodic theory to non periodic cases by following [9], [5], [12], and then by introducing, in the upscaling procedure, a preliminary step for clustering the flow regimes and decoupling the total flow upscaling from the upscaling of capillary effects.

In case of dominant convection we cannot expect that the upscaling problem will be reduced to only computing effective parameters or curves. The analysis of the linear one-phase flow problem, with a high global Péclet number, of order $1/\varepsilon$ like in [3] and [11], suggests that the form of the governing equations will also change, making upscaling more complicated than only seeking effective parameters. One possible cause for the instability of the so called *dynamic upscaling methods* [7], used in petroleum engineering, as we will see in Section 5, is certainly related to the inconsistency of seeking effective parameters and curves, in a situation where convection (also called viscous forces, in petroleum engineering) is dominant .

3 Effective equations

3.1 Equations

From [8] where mathematically rigorous upscaling was derived by means of homogenization theory using "global pressure" concept, or from [21] and [20], [17] or [4], where upscaling was done by formal asymptotic expansion and volume averaging, we know that when the global Péclet and Bond numbers are of order 1 the upscaled equations have the same structure as the equations at the local scale, with effective capillary pressure curve and effective absolute and relative permeabilities (in petroleum engineering these "effective" or "upscaled" curves are called "Pseudo" curves). Up-

scaled equations have then the form:

$$\langle\phi\rangle\frac{\partial S^*}{\partial t}+\operatorname{div}\mathbf{Q}_w^*=\langle F_w\rangle, \tag{10}$$

$$-\langle\phi\rangle\frac{\partial S^*}{\partial t}+\operatorname{div}\mathbf{Q}_{nw}^*=\langle F_{nw}\rangle, \tag{11}$$

$$\mathbf{Q}_w^*=-\lambda_w^*(S^*)(\nabla p_w^*-\rho_w\mathbf{g}), \tag{12}$$

$$\mathbf{Q}_{nw}^*=-\lambda_{nw}^*(S^*)(\nabla p_{nw}^*-\rho_{nw}\mathbf{g}), \tag{13}$$

$$p_c{}^*(S^*)=p_{nw}^*-p_w^*. \tag{14}$$

In these equations, $\langle\cdot\rangle=\frac{1}{|\Omega|}\int_\Omega\cdot dx$ and the effective mobilities $\lambda_\xi^*(S^*)$, $\xi\in\{w,nw\}$, and the effective capillary pressure $p_c^*(S^*)$, are computed by a procedure which will be described below.

Remark 1 In [8], the two-phase flow equations are first transformed using global pressure concept and then homogenization theory is applied, leading to upscaled equations in transformed form (see equations (4.10)–(4.15) in [8]). But, after standard separation of fast and slow variables and after transforming the effective equations back from the global pressure form to the phases-pressure form we obtain equations (10)–(14).

3.2 General Upscaling algorithm

In order to avoid technical complications here and subsequently we will assume that the domain Ω is a parallelepiped with edges parallel to the coordinate axes. From the experimental capillary pressure data $p_c^i(.)$ and irreducible saturations, $S_{i,M},S_{i,m}$, given in each rock-type subdomain Ω_i , we define two constants $p_{c,min}$ and $p_{c,max}$; $p_{c,min}<p_{c,max}$, by:

$$\max_{1\le i\le n}p_c^i(S_{i,m})=p_{c,max},\quad \min_{1\le i\le n}p_c^i(S_{i,M})=p_{c,min}. \tag{15}$$

Then we proceed in four steps.

Step 1 The effective capillary pressure p_c^* in (10)–(14) is defined in the following way: First, for each value of capillary pressure, $u\in(p_{c,min},p_{c,max})$, we obtain a piecewise constant distribution of the saturation $S^0=\sum_{i=1}^n S_i\chi_{\Omega_i}$, from the constant values S_i, solutions of

$$u=\sum_{i=1}^n p_c^i(S_i)\chi_{\Omega_i}(x),\quad \forall x\in\Omega. \tag{16}$$

Then, we set

$$p_c{}^*(S^*)=u,\quad S^*=\frac{\langle\phi S^0\rangle}{\langle\phi\rangle}. \tag{17}$$

Remark 2 Solvability of equation (16) is given by condition (15); and a unique effective capillary pressure curve is then defined. Moreover, it is easy to see that S^* is a smooth, decreasing function of u, and then ${p_c}^*$ still is a smooth decreasing function of S^*, $S^* \in [S^*_m, S^*_M]$, with

$$S^*_m = \frac{\langle \phi S_m \rangle}{\langle \phi \rangle}, \quad S^*_M = \frac{\langle \phi S_M \rangle}{\langle \phi \rangle}, \tag{18}$$

and

$$p^*_c(S^*_m) = p_{c,max}, \quad p^*_c(S^*_M) = p_{c,min}. \tag{19}$$

Step 2 Effective mobility tensors are defined by formula

$$\lambda^*_\alpha(S^*)\mathbf{e}_k = \langle \mathsf{K}\lambda_\alpha(\cdot, S^0)\nabla w^k_\alpha \rangle, \quad k = 1,2,3, \tag{20}$$

for $\alpha \in \{w, nw\}$; where according to the mathematical theory in [12] we may define function w^k_α from the usual closure problem in averaging method, as used in petroleum engineering [1], [13], [17].
Function w^k_α in (20) is a solution of the following auxiliary problem:

$$\begin{aligned} \operatorname{div}\left(\lambda_\alpha(x, S^0)\mathsf{K}(x)\nabla w^k_\alpha\right) = 0 \quad \text{in} \quad \Omega, \\ w^k_\alpha - x_k \quad \text{is periodic.} \end{aligned} \tag{21}$$

Saturation distribution S^0 in (20) and (21) is obtained from capillary pressure $u = p^*_c(S^*)$ by solving equation (16), as in Step 1.

Remark 3 For any value $S^*_m < S^* < S^*_M$, functions $\lambda_\alpha(x, S^0(x))$ are strictly positive and since permeability tensor K is positive definite it follows that auxiliary problems (21) are well posed and solutions w^k_α are unique up to an additive constant. Obviously this unknown additive constant does not influence the calculation of effective mobilities (20). Moreover, effective mobilities $\lambda^*_\alpha(S^*)$ as defined in (20) are symmetric positive definite tensors, monotone with respect to S^*; that is, for any S^* and $\overline{S}^*$, such that $S^* \leq \overline{S}^*$ we have

$$\lambda^*_w(S^*)\eta \cdot \eta \leq \lambda^*_w(\overline{S}^*)\eta \cdot \eta, \quad \lambda^*_{nw}(S^*)\eta \cdot \eta \geq \lambda^*_{nw}(\overline{S}^*)\eta \cdot \eta \quad \forall \eta \in \mathbb{R}^3.$$

This property can be easily established from an interpretation of the problem (21) as the Euler equation for minimisation of corresponding energy functional. Note finally that effective mobilities $\lambda^*_\alpha(S^*)$, having generally saturation dependent eigenvalues and eigenvectors, introduce saturation-dependent anisotropy into upscaled model.

Step 3 We introduce an effective absolute permeability K^*:

$$\mathsf{K}^*\mathbf{e}_k = \langle \mathsf{K}\nabla\varpi^k \rangle \tag{22}$$

where ϖ^k is a solution of the following auxiliary problem:

$$\begin{aligned} \operatorname{div}\left(\mathsf{K}\nabla\varpi^k\right) = 0 \quad \text{in} \quad \Omega \\ \varpi^k - x_k \quad \text{is periodic.} \end{aligned} \tag{23}$$

Remark 4 This effective absolute permeability K^* was defined in order to stay close to the classical two-phase flow model, and give to the effective equations (10)–(14) a form closer to the original equations (1)–(5)

Step 4 Effective relative permeability tensors $kr_w^*(S^*)$ and $kr_{nw}^*(S^*)$ are now defined from (20), (21) and (22), (23) as

$$kr_w^*(S^*) = \mu_w(\mathsf{K}^*)^{-1}\lambda_w^*(S^*), \quad kr_{nw}^*(S^*) = \mu_{nw}(\mathsf{K}^*)^{-1}\lambda_{nw}^*(S^*). \tag{24}$$

Remark 5 In general effective relative permeability tensors defined by (24) are full tensor and non symmetric, which could cause difficulties when using them in numerical simulations. But, it has been proved in [12], by using the theoretical framework of stochastic homogenization, that instead of imposing periodicity in auxiliary problems (21), and (23), corresponding to assumption of periodicity in homogenization, we may choose other boundary conditions in the auxiliary problems, some of them leading to effective mobility tensors with strongly dominant diagonal terms (see Subsection 4.1), more suitable for numerical simulations.

4 Numerical implementation

Local scale data are obtained geostatistically on a 3D "geological" grid which describes the porous domain geometry and its geological structure; however this fine scale description will be considered to be deterministic from the point of view of the numerical simulator, i.e. the grid block permeabilities and other parameters have no uncertainty associated with them. The block size l in that model is determined by the length of the geological heterogeneities, i.e. the "geological grid" size. We refer to the geological grid as *fine grid* and our aim is to build a *coarse grid* by aggregating fine grid blocks into larger, coarse blocks. The size of the coarse grid blocks is usually determined by the ability of multi-phase flow simulator.

Fine grid represents the local scale in our problem while the size of the coarse grid block represents global scale. Our upscaling method will be applied from fine grid to coarse grid blocks in order to associate to each coarse grid block effective values of porosity and permeability, effective relative permeability curves and effective capillary pressure curve. According to Remark 5 in upscaling algorithm steps 4, Subsection 3.2, we will prefer to use auxiliary problems leading to small extradiagonal terms in effective mobility tensors and in effective relative permeability curves.

4.1 Two Level Upscaling algorithm

From original upscaling algorithm of Subsection 3.2 we define now a two level upscaling procedure, one level is for upscaling total flow (one-phase rock parameters) and the second level is for upscaling capillary effects (relative permeability and capillary curves). Since the upscaling procedure will be run from the fine "geological" grid to either one or several coarse grid block (according the parameters or functions which are upscaled), for now on, Ω, will denote indistinctly any subdomain part of

all the geological domain, made at least of one coarse grid block and at most of the entire geological domain.

Step 1: Chose a priori a number of values of the capillary pressure u between $p_{c,min}$ and $p_{c,max}$ and for each u solve equation (16) which gives the distribution of saturation S^0 in Ω, corresponding to this u. For any value u and its corresponding S^0 compute the mean value S^*. The pair (S^*,u), represents then one point on the effective capillary pressure curve $u = p_c^*(S^*)$.

We proceed in that same way for each chosen value of the effective capillary pressure u in each Ω, and obtain discrete finite number of points of the effective capillary pressure curve.

Step 2: Diagonal effective mobility tensors are defined by formula:

$$\hat{\lambda}_\alpha^*(S^*)_{k,k} = \langle \lambda_\alpha(\cdot,S^0)\mathsf{K}\nabla w_\alpha^k \cdot \mathbf{e}_k \rangle, \quad k \in \{1,2,3\}, \tag{25}$$

for $\alpha \in \{w,nw\}$, where tensor $\hat{\lambda}_\alpha^*(S^*)$ replaces $\lambda_\alpha^*(S^*)$ from (12) and (13), and are computed not from (21) but by solving:

$$\begin{aligned} \operatorname{div}\left(\lambda_\alpha(x,S^0)\mathsf{K}(x)\nabla w_\alpha^k\right) = 0 \quad \text{in} \quad \Omega \\ w_\alpha^k = x_k \quad \text{on} \quad \mathscr{S}_k \\ \mathsf{K}(x)\nabla w_\alpha^k \cdot \nu = 0 \quad \text{on} \quad \partial\Omega\backslash\mathscr{S}_k; \end{aligned} \tag{26}$$

with S^0 computed as in Step 1 from $u = p_c^*(S^*)$, where $\mathscr{S}_k = \partial\Omega \cap \{x_k = const\}$; $k = 1,2,3$; $\alpha \in \{w,nw\}$ and ν denotes outer unit normal field.

Step 3: We proceed in a similar way with effective absolute permeability tensor; instead of (23), we solve:

$$\begin{aligned} \operatorname{div}\left(\mathsf{K}\nabla\varpi^k\right) = 0 \quad \text{in} \quad \Omega \\ \varpi^k = x_k \quad \text{on} \quad \mathscr{S}_k \\ \mathsf{K}\nabla\varpi^k \cdot \nu = 0 \quad \text{on} \quad \partial\Omega\backslash\mathscr{S}_k, \end{aligned} \tag{27}$$

for $k = 1,2,3$.
Then we define a diagonal effective permeability tensor by formula:

$$\hat{\mathsf{K}}_{k,k}^* = \langle \mathsf{K}\nabla\varpi^k \cdot \mathbf{e}_k \rangle, \quad k \in \{1,2,3\}. \tag{28}$$

Step 4: Directional effective relative permeability function, for k^{th} direction, is then

$$\hat{kr}_{\alpha,k}^*(S^*) = \mu_\alpha \frac{\hat{\lambda}_\alpha^*(S^*)_{k,k}}{\hat{\mathsf{K}}_{k,k}^*}, \quad \alpha \in \{w,nw\}. \tag{29}$$

Remark 6 Intrinsic permeability and porosity, which characterize the (total) flow regime, will be upscaled on geological zones associated to (total) flow regime zones defined at fine scale, using only step 3. Upscaling capillary effects (relative permeability and capillary curves) will be done independently, on larger porous domain according the level of the capillary forces, following steps 1, 2 and 4. Decoupling the

computation of effective one-phase flow parameters from the computation of effective two-phase saturation functions, is essential in this two level upscaling method, as illustrated in Subsection 6.3.

Remark 7 Assuming that $\phi(x)$, $\mathsf{K}(x)$, $kr_\alpha(x,S)$ and $p_c(x,S)$ are realizations of some statistically homogeneous random fields, it was shown in [9] that, in case of a unique rock-type, if the fields K and ϕ are ergodic then there exists a purely deterministic flow at global scale, associated to constant averaged porosity ϕ^{hom} and to constant homogenized tensor K^{hom}, which can be approximated either by means of (27), (28) or by means of (22), (23). Although, in both cases, averaged tensors K^* and $\hat{\mathsf{K}}^*$ in (22) or (28) are depending on realization Ω and its relative size L/l, it was shown in [12] that formula (22), with auxiliary problem (23), gives an approximation of real homogenized permeability tensor as well as formula (28), with auxiliary problem (27) in the sense that taking linear boundary conditions like the ones in (23) or in (27) does not influence the limits, $\mathsf{K}^* = \mathsf{K}^*(\Omega) \to \mathsf{K}^{hom}$ and $\hat{\mathsf{K}}^* = \hat{\mathsf{K}}^*(\Omega) \to \mathsf{K}^{hom}$, when the ratio l/L tends to 0. The same properties apply to the approximations λ_α^* and $\hat{\lambda}_\alpha^*$, given by (20) and (25), of the homogenized relative permeability curves.

Moreover, taking no-flux boundary conditions on $\partial\Omega \setminus \mathscr{S}_k$ in (26) (respectively in (27)) leads to gradients ∇w_α^k (respectively $\nabla \varpi^k$) which are oriented in the k-direction with negligible other directions components. As a major consequence, if Ω is sufficiently big, averaged tensors $\hat{\lambda}_\alpha^*$ in (25) (respectively $\hat{\mathsf{K}}^*$ in (28)) are then diagonal, or at least close to, with negligible, if not zero, extra-diagonal terms. Considering only the diagonal of the effective tensors could be then considered as a good approximation (similar to lumping).

Remark 8 Problems (26) and (27) are solved by mixed finite element method in order to make better approximation of the fluxes $\mathsf{K}\nabla w_\alpha^i$ and $\mathsf{K}\nabla\varpi^i$, which are averaged in formulas (25) and (28) .

Remark 9 The upscaling procedures described in Subsection 3.2 and in Section 4 computing respectively $(\mathsf{K}^*, \lambda_\alpha^*)$ and $(\hat{\mathsf{K}}^*, \hat{\lambda}_\alpha^*)$ have been implemented in the code *HomCode* and *JHomogenizer*, see [15] and [2]. Computational efficiency of the upscaling procedure is high regardless of the large number of local problems to be solved. This is due to the fact that the local problems are first linear and stationary, and thus easy to solve; and also are mutually independent then can be solved in parallel, in a preprocessing phase before the two-phase flow simulation itself.

5 Other upscaling methods

There is a number of others upscaling methods that can be found in engineering literature. Among them, the so called *dynamic methods* are supposed to do upscaling when the flow regime is characterized by a high Péclet number, $Pe_l = O(1)$ or even $Pe_l = O(1/\varepsilon)$. Dynamic methods are based on conservation of the fluid flow through Ω boundaries. To that aim, first a fine grid simulation is run; from which, at certain time intervals, the fluxes, pressures and saturations are written out for every fine grid block. Then the mean values of these quantities are computed in each Ω; and

the *Pseudo-functions* are finally computed by relating the flow rates to the pressure gradient, between neighboring Ω.

There are different dynamic methods which differ essentially by the way they average out different quantities. Dynamic methods and practical difficulties of their use are described in [7]. Here we have chosen the *pore volume weighted* [19] method (PVW in short), which is a version of the *Kyte and Berry* [16], and is already implemented in PSEUDO, [19]. It differs from the original Kyte and Berry algorithm only in the way of computing pressures.

An other method often used in engineering practice, and maybe the simplest method used for upscaling relative permeabilities, is the *dominant facies* method. It starts from an already upscaled absolute permeability tensor, computed according to procedure (27)-(28); and the *effective relative permeability curve*, in each coarse block Ω, is then taken equal to the relative permeability curve associated to the rock-type occupying the most of pore volume in Ω. Numerical experiment comparison of the two level upscaling method versus the PVW and the dominant facies (FD in short) methods will be presented in Subsection 6.6.1.

6 Numerical experiment results

In this section we want to compare different two-phase flow upscaling methods, used in engineering applications, to the two level upscaling method presented herein. Our goal is to compare their accuracy in a situation (geological and fluid data, numerical simulator and upscaling packages) synthesizing real upscaling problems encountered by engineers.

First, it was important to choose an upscaling package including some of the most popular two-phase flow upscaling methods in engineering; and do the numerical simulations with a widely used two-phase flow numerical simulator coupled with this upscaling package output. Our choice was then to use the upscaling package PSEUDO ([19]), and as numerical simulator ECLIPSE ([22]). Mainly because both PSEUDO and ECLIPSE are petroleum engineering oriented, we prefer to consider in our numerical comparison experiments an immiscible two-phase flow with water and oil phases.

Secondly, in order to make the comparison on a situation similar to the ones engineers are faced to, we are using a stochastic realization of a 3-D geostatistic simulator (TRIMOD) for generating a "synthetic" geological domain, G, of 10^3 square meters area by 40 meters high. This "synthetic" geological domain and the associated data generated on a fine "geological" grid are defining now a heterogeneous local scale model. All the considered upscaling methods will be applied to this same heterogeneous local scale model and give an upscaled model with data defined on coarser grids, i.e. at a global scale. Finally, we will compare numerical simulations, on all the entire geological domain G, using the same indicators (water cuts obtained at two locations P_1 and P_2, and oil production at location P_1), given by all the obtained "upscaled models" versus the simulations given by the original local scale model.

6.1 Fine grid data (local model)

The simulated geological domain, G, is a parallelepiped of $1000 \times 1250 \times 40$ meters discretized by a fine grid composed of 20 grid blocks in x-direction, 25 in y-direction and 20 in z-direction; all fine grid blocks have dimension $50 \times 50 \times 2$ meters and the total number of fine grid blocks is then 10000. Rock permeability and porosity were obtained from geostatistical simulations using TRIMOD:

1. Horizontal permeability k_h is a stationary random field realisation whose cumulative probability density F is given by the following table:

k (mD)	0	0.1	1	30	50	150	300	400	600
F	0	0.05	0.3	0.4	0.5	0.6	0.8	0.9	1

2. Vertical permeability k_v is obtained from the formula

$$\begin{cases} k_v/k_h = 0.1 & \text{for} \quad k_h > 10 \quad \text{mD}, \\ k_v/k_h = 0.01 & \text{for} \quad k_h \leq 10 \quad \text{mD}, \end{cases}$$

3. Porosity ϕ is given by

$$\phi = \begin{cases} 0.05 + 0.02345 \log(k_h) & \text{for} \quad \phi > 10^{-2}, \\ 10^{-2} & \text{otherwise.} \end{cases}$$

The fluid characteristics corresponding to the two phases are: $\mu_w = 0.32$ cP, $\mu_{nw} = 0.64$ cP; $\rho_w = 1150$ kg/m^3, $\rho_{nw} = 884$ kg/m^3; and the initial pressure is 284 bar at –1000 m (water-oil contact). For simplicity we assume that there are two different rock-types (two sets of relative permeability and capillary pressure curves), distributed in the entire geological domain according to horizontal absolute permeability k_h distribution: Denoting k_{moy} the mean value of k_h, then the rock-type of a given fine grid block has been set according to the rule

$$\begin{array}{c} \text{rock-type 1 if } k_h < k_{moy}\ , \\ \text{rock-type 2 if } k_h \geq k_{moy}\ . \end{array}$$

With this rock-type distribution finally we have 60 % of the rock-type 1, and 40% of the second rock-type in the entire geological domain, G,. Relative permeabilities and capillary pressure curves corresponding to each rock-type are given according to Figure 1. There are 4 injection wells, $I1, I2, I3$ and $I4$, working as water injectors, at constant rate of 100 m^3/day, in the four lowest layers of G: well $I1$ in block (5,14); well $I2$ in block (2,2); well $I3$ in block (19,13) and well $I4$ in block (8,23). There are two production wells, in the four upper layers of G: $P1$ and $P2$, working at constant rate of 200 m^3/day; well $P1$ in block (11,8) and well $P2$ in block (13,19).

6.2 Flow regime

As explained in Section 2 our upscaling method is theoretically founded for flow regime corresponding to global Péclet and Bond numbers of order 1. From the above data we have as characteristic numbers: L_h = 1000 m; L_v = 40 m; l_h = 50 m; l_v = 2

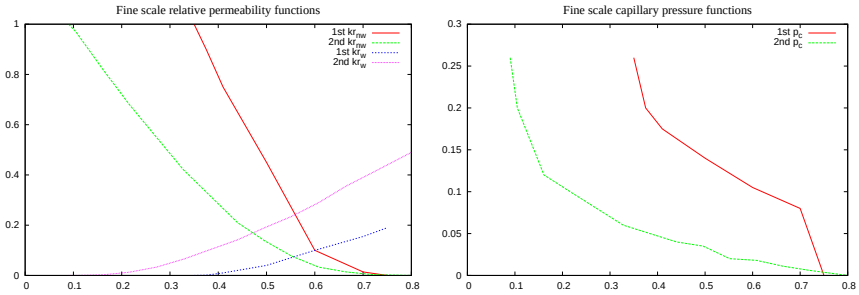

Fig. 1 The two sets of relative permeability functions and capillary pressures curves corresponding to the two rock-types on the fine grid blocks.

m; k_h^0 = 100 mD; k_v^0 = 10 mD; μ^0 = 0.5 cP; Pc^0 = 0.2 bar; $\rho^0 = \Delta\rho$ = 250 kg/m^3; g = 10 m/s^2. The characteristic mean velocity q^0 is estimated by dividing distance between two neighbouring wells (production well $P1$ and injection well $I1$) by the breakthrough time at the production well, giving in horizontal and vertical direction $q_h^0 < 0.28$ m/day, $q_v^0 < 2.4 \cdot 10^{-2}$ m/day. From these numbers by formulas (8), (9) we see that $\varepsilon \approx 0.05$, with horizontal local Péclet's number $Pe_l < 41$, vertical local Péclet's number $Pe_l < 1.4$ and local Bond's number $Bo_l \approx 0.25$. In some parts of the porous domain we could not exactly be under the assumption of dominating capillarity like in the horizontal direction where viscous forces are important since the maximum of Pe_l in the direction of the wells is $Pe_l \approx 41 \gg 1$. In vertical direction the capillary forces are more important than in horizontal direction due to lower permeability in that direction to and small thickness of the domain.

6.3 Coarse grid upscaled data and aggregation rates

At global scale the geological domain data are given on coarse grid blocks whose dimensions are given by aggregating the fine grid blocks along coordinate axes. At local scale the geological domain data characteristics were given on a fine grid, as described in Section 6.1, with 20 fine grid blocks in x-direction, 25 in y-direction and 20 in z-direction. We start by aggregating fine grid blocks uniformly by 4 in x-direction, by 5 in y-direction and by 4 in z-direction; this uniform aggregation rate is denoted $\mathscr{U}(4,5,4)$; each coarse grid block Ω consists then of $4 \times 5 \times 4 = 80$ fine grid blocks, and there are $5 \times 5 \times 5 = 125$ coarse grid blocks. In presence of two largely different time scales for diffusion and convection, in order to calculate correct mean values in steps 1, 2 and 3 of the Two Level Upscaling Algorithm, Section 4, we should introduce different levels of upscaling one for the total flow and another one for the capillary effects. It could happen then that the aggregation rate, used to capture the global effects of capillary pressure, is too big to take in account the total flow regime variations in different regions. Coarse grid blocks, Ω, used in upscaling total flow (calculation of effective absolute permeability in step 3) should be then smaller than the coarse grid blocks, Ω, necessary for upscaling capillary pressure and relative permeabilities. It is then necessary to use different coarse grid block sizes (or

aggregation rates), one size associated to global convective effects and an other size associated to global capillary pressure and relative permeabilities effects. Therefore, in the Two Level Upscaling Algorithm, Section 4, we will use different aggregation rates for upscaling capillary pressure and relative permeability curves (steps 1 to 4) and to upscale absolute permeability (step 3) and porosity.

In order to emphasize this difference in aggregation rates we use subscripts K to denote aggregation rate applied to one-phase flow characteristics (porosity or absolute permeability) and subscript Pc, to denote aggregation rate for two-phase flow characteristics (relative permeabilities and capillary pressure). For example, the aggregation rate $\{\mathscr{U}_K(4,5,4)+\mathscr{U}_{Pc}(20,25,5)\}$ means that we have used in one hand a uniform $\mathscr{U}(4,5,4)$ aggregation rate to compute effective absolute permeability and porosity, and in the other hand a uniform $\mathscr{U}(20,25,5)$ aggregation rate to compute effective relative permeabilities and effective capillary pressure. This last aggregation rate in particular means that in the geological domain, G, there are four effective functions sets associated to four "big" coarse grid blocks Ω (four horizontal layers). More precisely, for computing effective one-phase flow characteristics, fine grid blocks have been aggregated into coarse grid blocks according to the flow dynamics, after identifying spatial zones of similar total flow regime. Such a procedure, either performed manually or by specialized software tool, may then lead to non uniform aggregation rate for defining the one-phase flow global characteristics. To describe such coarse grid dimensions, we cannot use the same notations as above, and we rather give the way of aggregating the fine grid blocks along coordinate axes. For instance, in the numerical tests described in Subsection 6.6.1, we used $6\times5\times6=180$ coarse grid blocks for upscaling one phase flow data: aggregation being done in the x-direction, with successively 6 different ratio (3, 3, 2, 2, 5, 5); in the y-direction with 5 equal ratio (5, 5, 5, 5, 5); in the z-direction with successively 6 different ratio (2, 2, 2, 4, 5, 5). This non uniform aggregation rate is then denoted, in short, $\mathscr{N}(6\times5\times6)$.

In other tests from the same Subsection 6.6.1 we also mix uniform and non uniform aggregation rates such as $\{\mathscr{N}_K(6\times5\times6)+\mathscr{U}_{Pc}(20,25,5)\}$.

6.4 Numerical experiments

In the following we will use the name *heterogeneous simulation* for numerical flow simulation done at local scale with original local heterogeneous data on fine grid blocks. Flow simulation using upscaled data defined on coarse grid blocks, at global scale, will be termed *homogeneous simulation*, although the upscaled data could be different in each coarse grid block Ω, and then be globally heterogeneous.

In order to have the same amount of numerical dispersion both in homogeneous and heterogeneous simulations all numerical flow simulations are performed over the same numerical grid i.e. the initial fine scale grid. In this way when we compare homogeneous (coarse grid data) versus heterogeneous (fine grid data) simulations, we are really testing efficiency of the upscaling method without mixing it with any additional numerical effects. In other words, in homogeneous simulation we redistribute the upscaled values and curves on the fine initial grid blocks and we run numerical simulation on this fine grid. Furthermore, in order not to interfere with the well

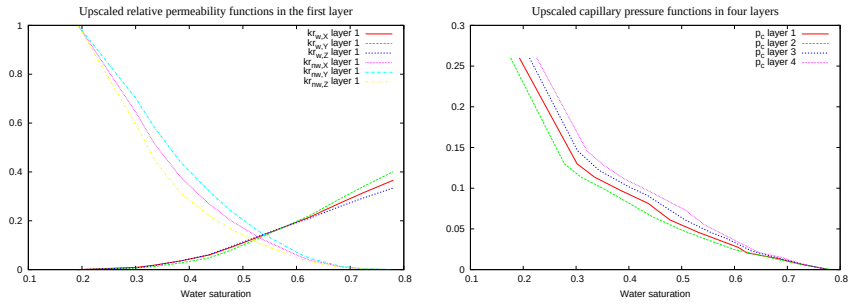

Fig. 2 Effective relative permeabilities, in the 3 directions, associated to the 1st layer. Effective capillary pressure curve , associated to each of the 4 layers. Effective curves are obtained by "two level upscaling" with uniform aggregation rate $\mathscr{U}(20,25,5)$.

model, we treat the boundary layer around each well by simply keeping the initial heterogeneities on the fine grid blocks all around the the perforated part of the well. All numerical tests presented herein were performed by ECLIPSE 100 simulator, [22].

6.5 Upscaled curves

According to the two level upscaling procedure, as described in Section 4, in each coarse grid block (global scale), starting from the heterogeneous data given on the fine grid blocks, we obtain three directional effective relative permeability curves for each phase, according to formula (29). As explained before in Subsection 6.3, since the capillary forces are weak, characteristic diffusion time τ_d is very big in the horizontal direction and we need to use large volumes in order to allow diffusive effects to take place; this is why we prefer to use a high uniform aggregation rate $\mathscr{U}(20,25,5)$ for saturation functions upscaling.

An example of effective functions obtained by two level upscaling on the coarse grid defined by this last aggregation rate is given in Figure 2. All the upscaled curves are built by interpolation from 12 computed saturation points, as described in Section 4, knowing that for each point we need to solve one auxiliary problem, (26). We notice, as can be seen from Figure 2, and according to the theory ([8], [21]), that the upscaled curves obtained by "two level upscaling" preserve monotonicity properties of rock-type curves.

Then for comparison purposes we have used the PVM method, in the package PSEUDO ([19]) for upscaling the saturation functions. Using the same fine grid block data (described in Subsection 6.1) and a uniform and moderate aggregation rate $\mathscr{U}(4,5,4)$, corresponding to $\{\mathscr{U}_K(4,5,4)+\mathscr{U}_{Pc}(20,25,5)\}$, by this method we generate 215 different pseudo-curves (of which we have kept only 89)! Rejection of pseudo curves was based on either insufficient number of points, or points being concentrated on a small part of the curve, or fairly high oscillations in the curve. They were simply replaced by curves corresponding to the dominating rock-type. We should also say that most of the accepted curves have been additionally "corrected" in

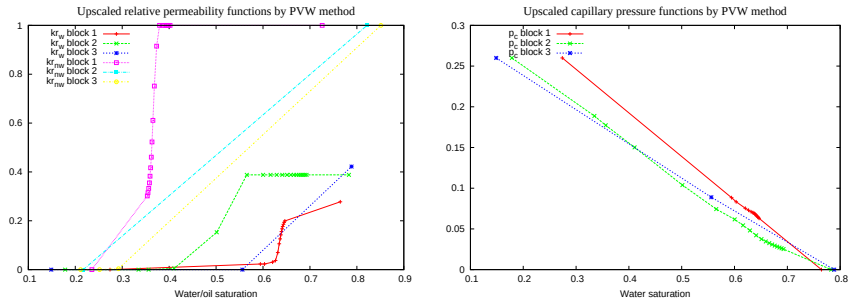

Fig. 3 Effective relative permeability and capillary curves obtained by the Pore Volume Weighted Method plus monotonicity correction, with a uniform aggregation rate $\mathscr{U}(4,5,4)$.

order to keep at least monotonicity. In Figure 3 we present just one set of the upscaled curves obtained by the PVW method plus monotonicity correction.

6.6 Comparison of different upscaling method results

6.6.1 Two level upscaling results

In the first test presented in Figure 4 we compare heterogeneous simulations computed from fine grid data (local scale parameters and curves) to homogeneous simulation computed from upscaled data (global scale parameters and curves) given by the two level upscaling method, on coarse grid blocks obtained by $\{\mathscr{U}_K(4,5,4) + \mathscr{U}_{Pc}(4,5,4)\}$ aggregation rate. In all forthcoming tests, like in Figure 4:

- As main indicators for the upscaling procedure quality, we take the well water cuts (WWCT) on both production wells $P1$ and $P2$, and the well oil production total (WOPT), for the production well $P1$ only.
- On the left, black and red curves correspond to water-cut on production well $P1$, computed respectively by homogeneous and heterogeneous simulations. Green and yellow curves correspond to water-cut on production well $P2$, computed respectively by homogeneous and heterogeneous simulations.
- On the right, the black curve corresponds to WOPT computed by homogeneous simulation and the red one to WOPT computed by heterogeneous simulation.

We see that the results presented in Figure 4 are not really satisfactory; particularly the difference in water-cut is important on both production wells. Reason for such difference is an inadequate upscaling of capillary effects due to the size of the coarse grid blocks which are too small compared to the characteristic capillary diffusion time in this example. In order to increase the volume in which the upscaling of the capillary effects is done, we should take bigger aggregation rates than the ones used for upscaling the total flow.

In Figure 5, we present the results obtained with a coarse grid made of only four horizontal layers, corresponding to a decoupled aggregation rate $\{\mathscr{U}_K(4,5,4) + \mathscr{U}_{Pc}(20,25,5)\}$. We see then in Figure 5 significant improvement after introducing

this two different levels of upscaling. But we note that there is still a difference in the production well $P1$ water-cuts. This is the result of upscaling the absolute permeability without taking in account possible changes in the total flow regime. Actually these results shown in Figure 5 used, for upscaling the absolute permeability, an a priory uniform aggregation rate, $\mathscr{U}_K(4,5,4)$, without taking into account the diversity of the total flow regime. Observation of flow dynamics in the initial heterogeneous simulation, computed from the fine grid data, shows that there is a highly permeable channel between the injection well $I1$ and the production well $P1$. In order to improve the results considering the production well $P1$ we use a non uniform aggregation rate, $\mathscr{N}_K(6\times5\times6)$ (as described in Subsection 6.3), adapted to the localization of this permeable channel. In Figure 6, we compare results of heterogeneous simulations to results of homogeneous simulations computed with upscaled parameters and curves obtained by two level upscaling using two different (non-uniform for the total flow and uniform the capillary effects) aggregation rates $\{\mathscr{N}_K(6\times5\times6)+\mathscr{U}_{Pc}(20,25,5)\}$. And, as expected, we see a real improvement (from Figure 5) in the upscaled behavior, specially for the production well $P1$ behavior .

6.6.2 Other upscaling methods results

In Figure 7 we test results of homogeneous simulations using upscaled parameters and curves given by the FD method (see Section 5 for definition). In this example, the upscaling of absolute permeability was done using the same method (step 3 in Section 4) and the same (uniform) aggregation rate ($\mathscr{U}_K(4,5,4)$) as the ones used in the previous subsection, 6.6.1. Same (uniform) aggregation rate ($\mathscr{U}_K(4,5,4)$) is also used for determining the dominant facies (dominating rock-type). These results could be certainly improved by using a non uniform aggregation rate for upscaling the absolute permeability, according to the total flow regime, like it was done for the two level upscaling method, in Section 6.6. But, in contrast to the two level upscaling, increasing too much the aggregation rate for determining dominant saturation functions (i.e. the upscaled functions) in the FD method, leads to incorrect estimations of the global capillary effects on these coarse grid blocks. As a consequence, the FD method will always end up with a large number of dominating functions (upscaled

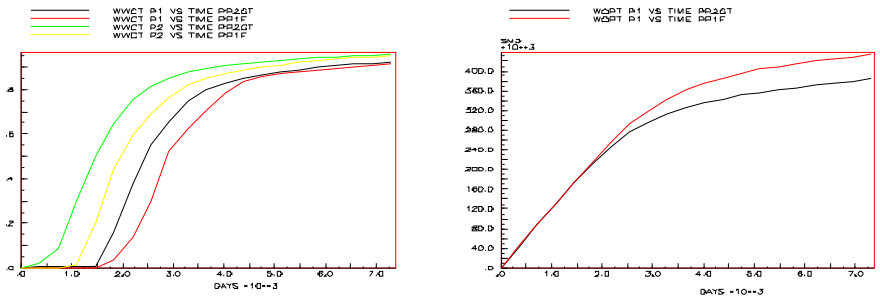

Fig. 4 Heterogeneous and homogeneous simulations based on the two level upscaling method, using the same uniform aggregation rate for upscaling total flow and capillary effects, $\mathscr{U}(4,5,4)=\{\mathscr{U}_K(4,5,4)+\mathscr{U}_{Pc}(4,5,4)\}$.

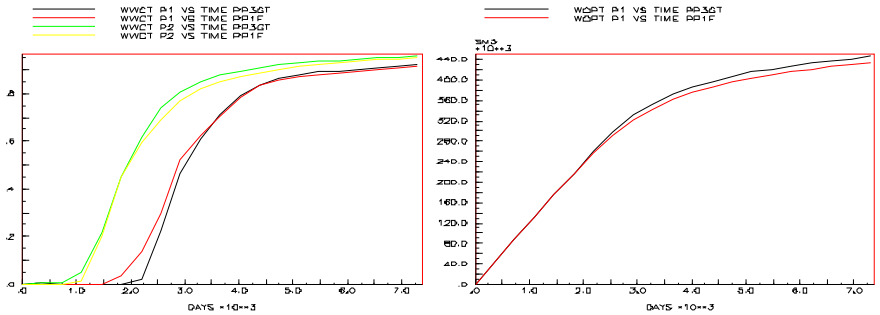

Fig. 5 Comparison of heterogeneous and homogeneous simulations based on two level upscaling method using two different uniform aggregation rates, for upscaling total flow and upscaling capillary effects: $\{\mathscr{U}_K(4,5,4)+\mathscr{U}_{Pc}(20,25,5)\}$.

functions), while the two level upscaling method gives a small number of different upscaled curves (only 4 in the example in Figure 6).

Finally we show in Figure 8 a numerical test using the pore volume weighting (PVW) method; the coarse grid is again obtained by the uniform aggregation rate $\mathscr{U}(4,5,4)$ for upscaling both total flow and relative permeabilities. The results are not really satisfactory, as expected from the upscaled curves obtained from this method and presented in Figure 3.

7 Conclusion

Numerical simulations, using the results of the two level upscaled method, show that if the local flow dynamics is taken into account in the choice of the coarse grid blocks on which the upscaling is done, and if the two-phase flow characteristics are upscaled on coarse grid blocks with dimensions consistent with the global diffusion time scale, then the so defined global flow is keeping the general physical flow characteristics and the main tendencies of the geology.

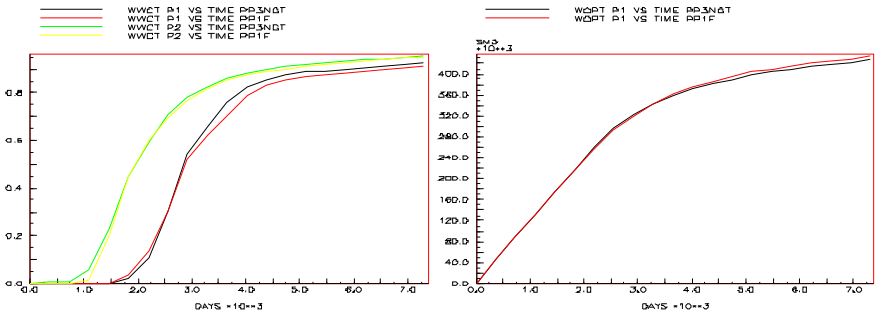

Fig. 6 Comparison of heterogeneous and homogeneous simulations based on two level upscaling method using a non uniform aggregation rate for upscaling the total flow and a uniform aggregation rate for upscaling the capillary effects: $\{\mathscr{N}_K(6\times5\times6)+\mathscr{U}_{Pc}(20,25,5)\}$.

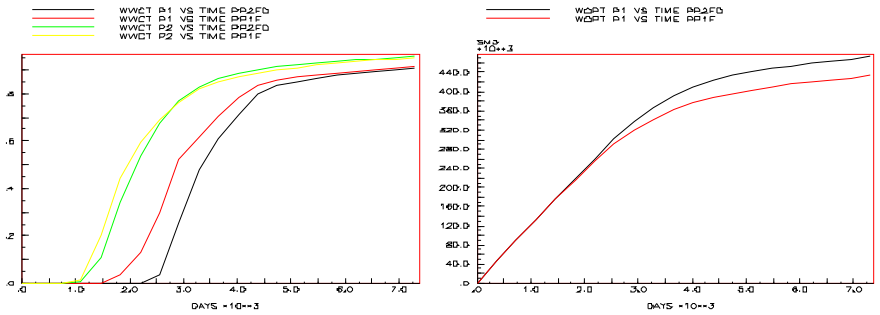

Fig. 7 Comparison of heterogeneous and homogeneous simulation based on upscaled data given by the dominant facies (FD) method, using one level of uniform aggregation rate, $\mathscr{U}(4,5,4)$.

Thanks to the decoupling of the upscaling level for one-phase rock parameters (porosity and rock permeability) from the upscaling level for two-phase rock functions, the *two level upscaling* method gives good results even in case of a relatively large Péclet number, i.e. outside the bounds imposed by the theoretical analysis in [8]. As explained in Section 6.3 this is due to the fact that: in the one hand we adapted the volume of averaging (the coarse grid block size) used for saturation functions to the diffusion time scale (defined in (8)), and in the other hand we adapted the choice of the coarse grid blocks, for upscaling the total flow, to the convection time scale (defined in (8)). The geological domain and the fluid characteristics used in the numerical experiments, presented herein, lead to a strong convection in the horizontal direction, but with the capillary forces staying relatively important in the vertical direction (smaller vertical Péclet's number). This is due to the fact that the thickness of the porous domain is small compared to the other dimensions. This is why we upscaled the capillary curves only in four horizontal layers, extending horizontally on all the domain; while we used smaller coarse blocks for upscaling the absolute permeability.

Moreover, we see on this example that our strategy leads to defining homogenized curves (p_c and kr_ξ), which are physically meaningful and defined on rather large volumes (capillary pressure being rarely dominant). Finally, for summarizing,

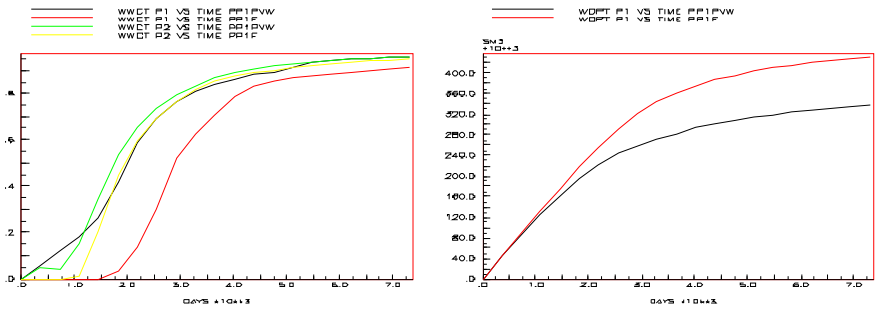

Fig. 8 Comparison of heterogeneous and homogeneous simulation based on upscaled data given by the Pore Volume Weighted (PVW) method, using one level of uniform aggregation rate, $\mathscr{U}(4,5,4)$.

the two-level upscaling method extends considerably the range of application of the upscaling method described in [4], [8], [17], [21] and compared to popular engineering methods (see [7], [16], [19]):

- leads to "pseudo functions" always consistent with the physical principles;
- gives only few different "pseudo functions"; preventing the use of any postprocessing technique for curve grouping, as for example clustering, which are not based on any physical ground.

Acknowledgements This work was partially supported by GdR MoMaS (PACEN/CNRS, ANDRA, BRGM, CEA, EDF, IRSN).

References

1. A. Ahmadi, M. Quintard, Large scale properties for two-phase flow in random porous media, Journal of Hydrology, Volume 183, Issues 1-2, August 1996, Pages 69-99.
2. B. Amaziane, A. Bourgeat, M. El Ossmani, M. Jurak and J. Koebbe, Homogenizer++: A platform for upscaling multiphase flows in heterogeneous porous media, Monografas del Seminario Matemtico Garca de Galdeano 33, 395402 (2006).
3. B. Amaziane, A. Bourgeat, M. Jurak, Effective Macrodiffusion in Solute Transport through Heterogeneous Porous Media SIAM J. on Multiscale Modeling and Simulation, Vol. 5, No. 1 ; pp. 184 - 204, 2004.
4. B. Ataie-Ashtiani, S. M. Hassanizadeh, M. Oostrom, M. A. Celia and M. D. White, Effective parameters for two-phase flow in a porous medium with periodic heterogeneities, J. Contaminant Hydrology, 49, 87-109, 2001
5. A. Badea, A. Bourgeat, Numerical simulation by homogenization of two phase flow through randomly heterogeneous porous media. Notes in Numerical Fluids Mechanics, vol. 59, Modeling and Computation in Environmental Sciences (1997), p. 13-24.
6. A. Badea, A. Bourgeat, Homogenization of Two-Phase Flow Through Randomly Heterogeneous Porous Media, International Conference on Mathematical Modeling of Flow through Porous Media, Saint-Etienne, 1995, Scientific World Pub., (1995), pp 44-58.
7. J. W. Barker, S. Thibeau, A Critical Review of the Use of Pseudorelative Permeabilities for Upscaling, SPE Reservoir Engineering, May 1997, pp 138-143.
8. A. Bourgeat, A. Hidani, Effective Model of Two-Phase Flow in a Porous Medium Made of Different Rock Types, Applicable Analysis, 58, (1995), pp 1-29.
9. A. Bourgeat, S. Kozlov, A. Mikelić, Effective Equations of Two-Phase Flow in Random Media, Cal. Variations and P.D.E., 3, (1995), pp 385-406.
10. A. Bourgeat, M. Jurak, F. Smaï, Two phase partially miscible flow; application to gas migration in a nuclear waste repository, arXiv:0802.4389v1.
11. A. Bourgeat, M. Jurak, A. Piatnitski, Averaging a transport equation with small diffusion and oscillating velocity; Math. Meth. Appli. Sci., Vol. 26, No. 2, 2003, pp. 95-117.
12. A. Bourgeat, A. Piatnitski, Approximation of effective coefficients in stochastic homogenization. Annales de l'Institut Henri Poincaré, Probabilités et Statistiques - PR 40 (2004), pp. 153-165.
13. A. Bourgeat, M. Quintard, S. Whitaker, Eléments de comparison entre la methode d'homogénéisation et la prise de moyenne avec fermature, CRAS, Paris, t. 306, serié II, pp. 463-466, 1998.
14. G. Chavant, J. Jaffre, Mathematical Models and Finite Elements for the Reservoir Simulations, Studies in Mathematics and its Applications, North-Holland, vol. 17, 1986.
15. J. Koebbe, HomCode and JHomogenizer, http://www.math.usu.edu/ koebbe/wwwHomog/index.html
16. J. R. Kyte, D. W. Berry, New Pseudofunctions to Control Numerical Dispersion, SPEJ (August 1975) 269.
17. D. Lasseux, M. Quintard, S. Whitaker, Determination of permeability tensors for two-phase flow in heterogeneous porous media: Theory, Transport in Porous Media, **24**: 107-137, 1996.
18. M. Panfilov, S. Oladyshkin, Limit thermodynamic model for compositional gas-liquid systems moving in a porous medium, Transport in Porous Media, **70**: 147-165, 2007.

19. PSEUDO Reference Manual, Intera Information Technologies Ltd.
20. M. Quintard, S. Whitaker, Two-Phase Flow in Heterogeneous Porous Media I: The influence of large spatial and temporal gradients, Transport in Porous Media, **5**: 341-379, 1990.
21. A. E. Saez, C. J. Otero, I. Rusinek, The effective Homogeneous Behavior of Heterogeneous Porous Media, Transport in Porous Media, **4**: 213-238, 1989.
22. Schlumberger ECLIPSE Technical Description 2005 A, Schlumberger.
23. ANDRA, Couplex-gaz, http://www.andra.fr/interne.php3?id_article=913&id_rubrique=76